Journal Pre-proof

The *Fusarium* mycotoxin, 2-Amino-14,16-dimethyloctadecan-3-ol (AOD) induces vacuolization in HepG2 cells

A Solhaug, ML Torgersen, JA Holme, J Wiik-Nilsen, B Thiede, GS Eriksen

PII: S0300-483X(20)30044-5

DOI: https://doi.org/10.1016/j.tox.2020.152405

Reference: TOX 152405

To appear in: *Toxicology*

Received Date: 23 December 2019

Revised Date: 3 February 2020

Accepted Date: 6 February 2020

Please cite this article as: Solhaug A, Torgersen M, Holme J, Wiik-Nilsen J, Thiede B, Eriksen G, The *Fusarium* mycotoxin, 2-Amino-14,16-dimethyloctadecan-3-ol (AOD) induces vacuolization in HepG2 cells, *Toxicology* (2020), doi: https://doi.org/10.1016/j.tox.2020.152405

The *Fusarium* mycotoxin, 2-Amino-14,16-dimethyloctadecan-3-ol (AOD) induces vacuolization in HepG2 cells.

A Solhaug[1*], ML Torgersen[2], JA Holme[3], J Wiik-Nilsen[1], B Thiede[4], GS Eriksen[1]

[1]*Chemistry and Toxinology Research group, Norwegian Veterinary Institute, 0454 Oslo, Norway*

[2]*Department of Molecular Cell Biology, Institute for Cancer Research, the Norwegian Radium Hospital, Oslo University Hospital, 0379 Oslo, Norway*

[3]*Department of Environmental Health, Division of infection Control and Environment and Health, Norwegian Institute of Public Health, 0403 Oslo, Norway*

[4]*Department of Biosciences, University of Oslo, 0316 Oslo Norway*

[*]Corresponding author:

Anita Solhaug, PhD

Norwegian Veterinary Institute,

P.O.BOX 750 Centrum, 0106 Oslo, Norway

Tel: +47 23216214; Fax: +47 23216201

E-mail: Anita.Solhaug@vetinst.no

Graphical abstract

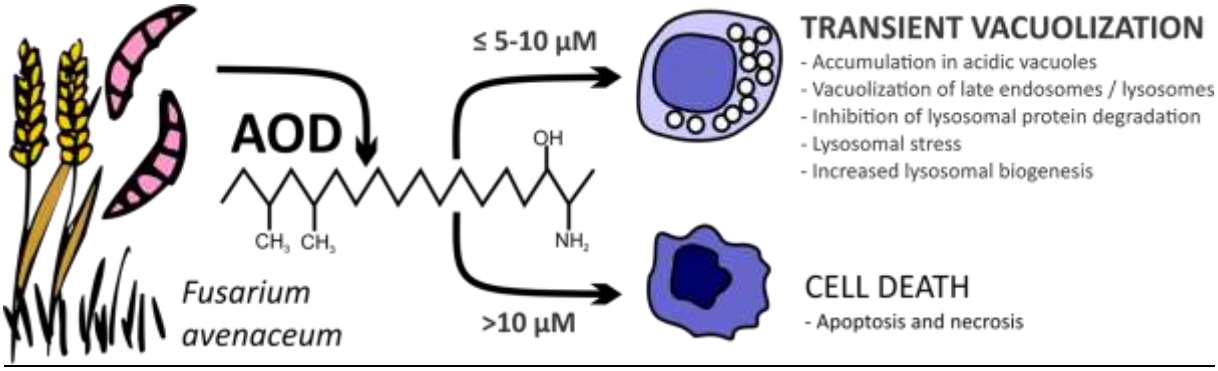

Highlights:

- AOD induced transient vacuolization in HepG2 cells
- The vacuolization was not linked to cell death processes
- The vacuolization was dependent on acidic lysosomes
- Inhibition of endosomal protein degradation and autophagy
- Vacuolization originates from disorders of the endolysosomal processeses

Abstract

The mycotoxin 2-Amino-14,16-dimethyloctadecan-3-ol (AOD) has been isolated from cultures of the fungus *Fusarium avenaceum*, one of the most prevalent *Fusarium* species. AOD is an analog of sphinganine and 1-deoxysphinganine, important intermediates in the *de novo* biosynthesis of cellular sphingolipids. Here we studied cellular effects of AOD using the human liver cell line HepG2 as a model system. AOD (10 µM) induced a transient accumulation of vacuoles in the cells. The effect was observed at non-cytotoxic concentrations and was not linked to cell death processes. Proteomic analyses indicated that protein degradation and/or vesicular transport may be a target for AOD. Further studies revealed that AOD had only minor effects on the initiation rate of macropinocytosis and autophagy. However, the AOD-induced vacuoles were lysosomal-associated membrane protein-1 (LAMP-1) positive, suggesting that they most likely originate from lysosomes or late endosomes. Accordingly, both endosomal and

autophagic protein degradation were inhibited. Further studies revealed that treatment with concanamycin A or chloroquine completely blocked the AOD-induced vacuolization, suggesting that the vacuolization is dependent of acidic lysosomes. Overall, the results strongly suggest that the increased vacuolization is due to an accumulation of AOD in lysosomes or late endosomes thereby disturbing the later stages of the endolysosomal process.

Keywords: Emerging mycotoxins; sphingolipids; vacuolization; endosomes; lysosomes

Graphical abstract:

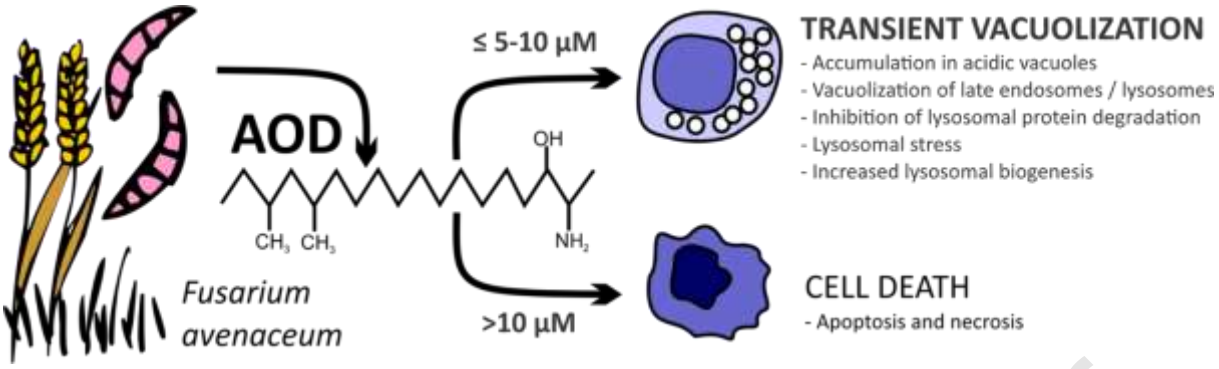

Keywords: Emerging mycotoxins, sphingolipids, vacuolization, endosomes, lysosomes

Highlights:

- AOD induced transient vacuolization in HepG2 cells
- The vacuolization was not linked to cell death processes
- The vacuolization was dependent on acidic lysosomes
- Inhibition of endosomal protein degradation and autophagy
- Vacuolization originates from disorders of the endolysosomal processeses

Abbreviations:

Amino-14,16-dimethyloctadecan-3-ol (AOD), bovine serum albumin (BSA), ceramide synthase (CerS), cholera toxin subunit B (CT-B), chloroquine (CQ), concanamycin (Con A), 4′,6-diamidino-2-phenylindole (DAPI), dimethyl sulfoxide (DMSO), excitation (Ex), fetal bovine serum (FBS), human hepatocellular carcinoma derived cells (HepG2), lysosomal-associated membrane protein-1 (LAMP-1), emission (Em), microtubule-associated protein 1 light chain 3 (LC3B), Modified Eagle Medium Eagle (EMEM).

1. Introduction

Mycotoxins are secondary metabolites produced by different mold fungi. Contamination of agricultural crops by fungi and their associated mycotoxins is a serious problem worldwide. Some mycotoxins are potent toxins naturally occurring in cereal and cereal-based food. The fungal metabolite, 2-Amino-14,16-dimethyloctadecan-3-ol (AOD, Figure 1) was isolated as a cytotoxic compound from a rice culture of *Fusarium avenaceum* in 2005 (Uhlig et al. 2005). *F. avenaceum* is one of the most prevalent *Fusarium* species found in cereals all over Europe, especially in Scandinavia. Even though the fungus can produce AOD in mg/g amounts under laboratory conditions (Uhlig et al. 2005), extensive surveys on its natural occurrence have not yet been carried out. During a pilot study on Norwegian grain (Uhlig et al. 2013), AOD was detected in 35 and 36% of the samples with maximum concentrations of 10.8 and 2.46 mg/kg in barley and wheat samples respectively, demonstrating its relevance as a contaminant of field grain. AOD is found to be cytotoxic in the human hepatocellular carcinoma derived cells (HepG2) (Ivanova and Uhlig 2008) and THP-1 monocytes (Solhaug et al. 2016), however, the exact mechanism leading to the cytotoxicity is unknown. AOD has structural features of the mammalian sphingoid bases sphinganine and 1-deoxysphinganine (Zitomer et al. 2009) as well as the mycotoxin and well-known ceramide synthase (CerS) inhibitor fumonisin B1 (Riley and Merrill 2019) (Figure 1).

Sphingolipids are both structural components of cell membranes and bioactive molecules (Kitatani et al. 2008). Sphinganine and sphingosine (Figure 1) are important components of cellular sphingolipid metabolism. Disruption of sphingolipid metabolism has been shown to cause disease in farm and laboratory animals and has been associated with a variety of human diseases (Riley and Merrill 2019). Sphingolipids have a central role in regulation of the inflammatory response. They are involved in control of leukocyte activation and migration, and are recognized as essential players in host response to pathogenic infection

(Chiricozzi et al. 2018). Furthermore they are involved in a number of inflammatory diseases including neurodegeneration (Pujol-Lereis 2019), cancers (Hait and Maiti 2017; Lai et al. 2019) atherosclerosis (Hornemann and Worgall 2013) and are linked to the development of neural tube defects (Lai et al. 2016; Marasas et al. 2004). Recent studies have also revealed that lipids including phospholipids, sphingolipids and sterols play an important role in autophagosome formation (Martens et al. 2016). Furthermore, there are studies linking autophagy to these diseases and several studies suggest that the mechanism involved in some of the toxic effects of sphingolipids is through their effects on autophagy (Cecconi et al. 2008; Grootaert et al. 2018; Lai et al. 2019; van Echten-Deckert and Alam 2018).

Recent studies report that mycotoxins such as patulin (Guo et al. 2013), zearalenone (Wang et al. 2014) and alternariol (Solhaug et al. 2014) are linked to autophagy. It is well known that autophagy can be stimulated by various forms of cellular stress, including lipid interactions, protein aggregation and DNA damage (Kroemer et al. 2010; Young et al. 2013). Different forms of autophagy have been described: macroautophagy, chaperone mediated autophagy and microautophagy. Macroautophagy, commonly only called autophagy, involves packing of damaged cell components within membrane structures (autophagosomes) that subsequently fuse with lysosomes thereby forming an autolysosome (Breiden and Sandhoff 2019). More specifically, phospholipids and sphingolipid catabolism and inherited sphingolipidoses are found to be of great importance for lysosomal function and physiological lipid turnover (Grassi et al. 2019; Kitatani et al. 2008; Thelen and Zoncu 2017). Lysosomes are the terminal degradative compartment not only for autophagy, but also for endocytosis (Inpanathan and Botelho 2019). Endocytosis pathways can be subdivided into four categories: receptor-mediated endocytosis (also known as clathrin-mediated endocytosis), caveolae-mediated endocytosis, pinocytosis and phagocytosis. Similar to autophagosomes the endocytic vesicles

formed will fuse with the lysosome. Recently, sphingosine was similarly reported to as a critical metabolite in endocytic trafficking (Young et al. 2016).

In the present study, we report that treatment with AOD results in accumulation of vacuoles in HepG2 cells. Proteomic analyses of exposed cells suggested that AOD affected various parts of the vesicular transport system. This was further substantiated by detailed studies revealing that vacuole formations was due to a temporary disturbance of the endolysomal degradation pathway.

2. Materials and methods

2.1. Reagents and chemicals

4′,6-Diamidino-2-phenylindole (DAPI), Vybrant lipid raft labelling kit, lysosensor DND-160, lysotracker red DND-99, mitotracker red CMXRos, DQ red BSA, ProLong gold antifade reagent, collagen I rat tail, pierce ECL western blotting substrate, Alamar Blue, halt proteinase inhibitor cocktail, gels and buffers for western blotting (NuPAGE system) were all purchased from Thermo Fisher (Carlsbad, CA, USA). Lysis buffer (#9803), phosphatase inhibitor cocktail, non-fat dry milk, normal goat serum, rapamycin, LC3B antibody (#3868), P-mTOR antibody (Ser2448, #5536), P-S6K antibody (Thr389, #9205), β-actin-HRP antibody (#5125) and anti-rabbit IgG HRP-linked antibody were from Cell Signaling (Beverly, MA, USA). LAMP-1 antibody (H4A3, #sc2001) was from Santa Cruz Biotechnology (Dallas, Texas, USA). Modified Eagle Medium Eagle (EMEM), phosphate buffered saline (PBS), penicillin/streptomycin, glutamine and fetal bovine serum (FBS; EU standard) were from Lonza (Verviers, Belgium). Bio-RAD DC protein assay was from Bio-Rad Laboratories Inc (Hercules, CA, USA). Chloroquine (CQ), monesin, nigericin, Oil Red O, trypsin-EDTA solution (2.5 g/L) and dimethyl sulfoxide (DMSO) and bovine serum albumin (BSA) were from Sigma-Aldrich (St.Louis, MO, USA). Millicell EZ slide (Millipore). CellTox Green

cytotoxicity assay, caspase-glo 3/7 assay were from Promega (Madison, WI, USA), p62 antibody (#GP62-C) was purchased from Progen Biotechnik (Heidelberg, Germany). Anti-guinea pig IRDye 680RD (#68077) was from LICOR (Lincole, NE, USA). 2-amino-14.16-dimethyloctadecan-3-ol (AOD) was purified by Silvio Uhlig (98% purity) as described in Uhlig et al. (2005).

2.2. Cell culture and treatments

The HepG2 cell line (Human Caucasian hepatocyte carcinoma) was obtained from the European Collection of Cell Cultures (ECACC), and grown in EMEM supplemented with 1% glutamine, 10% FBS and 1% penicillin/streptomycin. The cells were cultured at 37°C under 5% CO_2 in a humidified incubator and sub-cultivated twice a week by trypsination. The cells were plated on collagen coated plates (collagen 1, rat tail), 90 000 cells/cm^2 the day before experiments. AOD was dissolved in DMSO and the final concentration of DMSO in cell culture was 0.2%. Appropriate controls containing the same amount of DMSO were included in each experiment. When inhibitors were used, the cells were pre-incubated 30 min with inhibitors before AOD exposure.

The very limited occurrence data indicate that AOD are present in barley and wheat at similar range as the well-studied mycotoxin deoxynivalenol (Uhlig et al. 2013). AOD is found to be cytotoxic in the similar range as deoxynivalenol (Maresca 2013) and similar concentrations (5-20 µM) are used in this study.

2.3 Transmission electronic microscopy

The cells were plated on transwell inserts (90 000 cells/cm^2). After exposure, the cells were washed once in PBS and fixed in 4% paraformaldehyde for 15 min at room temperature, washed with 0.1 M sodium cacodylate buffer, embedded in 3% low-melting agarose and post-fixed in

1% osmium tetroxide in 0.1 M sodium cacodylate buffer for 2 h. Subsequently, the cells were washed thoroughly in 0.1 M sodium cacodylate buffer, dehydrated with 10 min steps in ascending ethanol series (50–100%) and embedded in LR White resin (London Resin Company, EMS, England). Ultrathin sections were obtained using a Leica EM UC6 Ultramicrotome. The sections were stained with 4% uranyl acetate and 1% potassium permanganate for 10 min and examined and photographed using a FEI Morgagni 268 transmission electron microscope at the Imaging Centre, Norwegian University of Life Sciences.

2.4 Cytotoxicity

Alamar Blue assay*:* Metabolic activity of the cells was measured using the Alamar Blue assay according to the manufacturer's protocol. The dark blue oxidized form of Alamar Blue is reduced to a highly fluorescent form and the measured fluorescence intensity is thus proportional to the number of viable cells. The fluorescence, excitation (Ex) 555 nm/emission (Em) 585 nm) was quantified using Spectramax i3x plate reader (Molecular Devices, San Jose, Ca, USA). **CellTox™ Green:** CellTox™ Green is a non-toxic dye that stains DNA of cells with impaired membrane integrity. The binding interactions with DNA produce a fluorescence signal that is proportional with cytotoxicity (necrotic, late apoptotic cells). CellTox™ Green Dye was added to the cells as described by the manufacturer (Promega) and fluorescence (Ex485 nm/Em520 nm) quantified by Spectramx i3x plate reader, 40 different points/well (scan well) were read. **Caspase 3/7 assay:** The Caspase-Glo® 3/7 glo Assay was performed according to the manufacturer (Promega), and the obtained luminescent signals were quantified by using the Spectramx i3x plate reader.

2.5 Proteomic

The cells were plated on collagen-coated dishes (90 000 cells/cm^2) and exposed to AOD (5 or 10 µM) for 6 h. After exposure, the cells were lysed in lysis-buffer supplemented with 1% SDS, phosphatase inhibitor cocktail and halt proteinase inhibitor cocktail. The samples were then centrifugated (10 000 x g, 1 min) through a QIAshredder (Qiagen) for homogenization. The protein concentrations were quantified by using Bio-Rad DC protein assay kit. Lysed samples were frozen and stored in liquid nitrogen until analysis. Four volumes of ice-cold acetone were added to the thawed samples, vortexed and precipitated at -20°C overnight. Samples were centrifuged at 16 000 x *g* for 20 min at 4°C and the supernatant was discarded. Proteins were re-dissolved in 50 µl 6 M urea and 100 mM ammonium bicarbonate, pH 7.8. For reduction and alkylation of cysteines, 2.5 µl of 200 mM DTT in 100 mM Tris-HCl, pH 8 was added and the samples were incubated at 37°C for 1 h followed by addition of 7.5 µl 200 mM iodoacetamide for 1 h at room temperature in the dark. The alkylation reaction was quenched by adding 10 µl 200 mM DTT at 37°C for 1 h. Subsequently, the proteins were digested with 10 µg trypsin GOLD (Promega, Madison, WI, USA) for 16 h at 37°C. The digestion was stopped by adding 5 µl 50 % formic acid and the generated peptides were purified using OMIX C18, 10 µl (Agilent, Santa Clara, CA, USA), and dried using a SpeedVac concentrator (Concentrator Plus, Eppendorf, Hamburg, Germany). The tryptic peptides were dissolved in 10 µl 0.1% formic acid/2% acetonitrile and 5 µl of AOD treated samples was analyzed using an Ultimate 3000 RSLCnano-UHPLC system connected to a Q Exactive mass spectrometer (Thermo Fisher Scientific, Bremen, Germany) equipped with a nano-electrospray ion source. A lower injection volume (1.7 µl) of the control samples were injected to compensate for the higher protein concentrations. For liquid chromatography separation, an Acclaim PepMap 100 column (C18, 2 µm beads, 100 Å, 75 µm inner diameter, 50 cm length) (Dionex, Sunnyvale CA, USA) was used. A flow rate of 300 nL/min was employed with a solvent gradient of 4-35% B in 180 min.

Solvent A was 0.1% formic acid and solvent B was 0.1% formic acid/90% acetonitrile. The mass spectrometer was operated in the data-dependent mode to automatically switch between MS and MS/MS acquisition. Survey full scan MS spectra (from m/z 400 to 2000) were acquired with the resolution R = 70 000 at m/z 200, after accumulation to a target of 1e6. The maximum allowed ion accumulation times were 60 ms. This method allowed sequential isolation of up to the ten most intense ions, depending on signal intensity (intensity threshold 1.7e4), for fragmentation using higher-energy collisional induced dissociation (HCD) at a target value of 1e5 charges, NCE 28, and a resolution R = 17 500. Target ions already selected for MS/MS were dynamically excluded for 30 sec. The isolation window was m/z = 2 without offset. For accurate mass measurements, the lock mass option was enabled in MS mode.

Data were acquired using Xcalibur v2.5.5 and raw files were processed to generate peak list in Mascot generic format (*.mgf) using ProteoWizard release version 3.0.331. Database searches were performed using Mascot in-house version 2.4.0 to search the SwissProt database (Human, 20,279 proteins) assuming the digestion enzyme trypsin, at maximum one missed cleavage site, fragment ion mass tolerance of 0.05 Da, parent ion tolerance of 10 ppm, carbamidomethylation of cysteines as fixed modification, and oxidation of methionines, and acetylation of the protein N-terminus as variable modifications. Scaffold (version Scaffold_4.4.8, Proteome Software Inc., Portland, OR) was used to validate MS/MS based peptide and protein identifications. Peptide identifications were accepted if they could be established at greater than 95.0% probability by the Scaffold Local FDR algorithm. Protein identifications were accepted if they could be established at greater than 99.9% probability and contained at least one identified peptide (FDR < 1%). For quantitative data analysis, protein data from cells exposed to 5 or 10 µM AOD were compared to controls separately using t-test and p value of $p < 0.01$. The weighted spectral counts were compared between the three different groups using a significance level of $p < 0.01$. (Supplementary, proteomic data).

We performed a gene ontology enrichment analysis of the differentially expressed proteins using the Gene Ontology Consortium platform and the Panther Analysis tool (http://geneontology.org). In order to identify cellular targets and metabolic pathways affected by AOD, we inserted the list of differentially expressed proteins above the threshold of 2-fold altered protein expression into the following softwares; reactome.com (May 2019), gene onthology (May 2019), Panther (May 2019) and DAVID 6.8 (using the update from March 2016).

2.6 Lipid microdomains

The cells were plated on coated EZ microscopy slides (90 000 cells/cm^2). The cells were stained for lipid microdomains (lipid rafts) using cholera toxin subunit B (CT-B) conjugated to Alexa Fluor 488. To avoid internalization of the CT-B (Blank et al. 2007), the cells were fixed before staining. After treatment with AOD, the cells were washed once in PBS and fixed in 4% paraformaldehyde for 15 min at room temperature. The cells were then washed 3 times with PBS and blocked in 5% normal goat serum/PBS for 60 min at room temperature followed by incubation with CT-B Alexa Fluor 488 (1:2000) in blocking buffer for 60 min at room temperature. The cells were then again washed 3 times with PBS, the nuclei stained with DAPI (1:5000) for 5 min, and coverslips mounted with prolong. Confocal fluorescence microscopy was performed using a Zeiss LSM710 confocal microscope.

2.7 Macropinocytosis

The cells were plated on coated EZ microscopy slides (for microscopic analysis) or coated black 96-well plates with clear bottom (for plate reader quantification). The day after plating the medium was replaced with media containing Lucifer yellow (0.5 mg/mL) and AOD (10 µM) and incubated further for 6 h. The cells were then washed once in PBS, fixed in 4%

paraformaldehyde at room temperature for 15 min and again washed twice with PBS. For microscopic analysis the coverslips were mounted with ProLong® mounting medium before the microscopic analysis (Zeiss LSM710). For plate reading quantification the fluorescence (Ex440 nm/Em550 nm) was quantified using Spectramax i3x plate reader, 40 different points/well (scan well) were read.

2.8 Lysosomal staining and lysosomal pH

For microscopic characterization of the lysosomes, the cells were plated on coated EZ microscopy slides. After treatment with AOD, the cells were incubated with 50 nM lysotracker red diluted in the culture medium for 15 min, washed twice in PBS and fixed in 4% paraformaldehyde for 15 min, the cells were then washed again, the nuclei stained with DAPI (1:5000) for 5 min and coverslips mounted with ProLong® mounting medium. Confocal fluorescence microscopy was performed using a Zeiss LSM710 microscope. For quantification, the cells were plated on coated black 96-well plates with clear bottom. After AOD exposure, the cells were stained with lysotracker red (50 nM, 15 min), washed once in PBS, fixed in 4% PFA at room temperature for 15 min and again washed twice with PBS. The fluorescence was measured using Ex570 nm/Em590 nm. The Spectramax i3x plate reader were used for the measurements, and 40 points/well (scan well) were read.

Lysosomal pH was measured as described in (Coffey et al. 2014) using the dye lysosensor Yellow/Blue DND-160. In brief, the cells were incubated with 2 µM lysosensor yellow/blue DND-160 in complete culture medium for 5 min, 37°C before the cells were gently washed 3 times with PBS. The fluorescence was measured using Ex340 nm/Em440 nm and Ex380 nm/Em535 nm. Lysosomal pH was determined from the ratio of Ex440 nm/Em535 nm. The Spectramax i3x plate reader were used for the measurements, and 40 points/well (scan well) were read. The absolute pH levels were obtained by loading the cells with lysosensor as

described above, and the lysosomal pH was equalized by incubating the cells in calibration buffer (20 mM MES (2-(N-morpholino)ethanesulfonic acid), 110 mM KCl, 20 mM NaCl, 15 µM monesin, 30 µM nigericin) at pH values of 4.0, 4.5, 5.0, 5.5 and 6.0 for 15 min at 37°C. The cells were then read with a plate reader as described above. The calibration curve is shown in supplementary Figure S6.

2.9 Immunostaining and microscopic characterization of LC3B and LAMP-1

For LC3B immunofluorescence analysis the cells were plated on coated EZ microscopy slides. After treatment the cells were washed in PBS, fixed and permeabilized in ice cold methanol (100%), followed by blocking in 5% normal goat serum in PBS for 1 h at room temperature. The cells were then stained with anti-LC3B (1:200) diluted in antibody staining buffer (1% BSA/PBS, 0.05% saponin) over night at 4°C. The cells were then rinsed 3 times in PBS and incubated with secondary antibody conjugated to Alexa Fluor 488 diluted in antibody staining buffer for 2 h at room temperature. The cells were then again washed 3 times with PBS, the nuclei stained with DAPI (1:5000) for 5 min, and coverslips mounted with ProLong® mounting medium. Confocal fluorescence microscopy was performed using a Zeiss LSM710 microscope.

For LAMP-1 immunofluorescence analysis in combination with Lucifer yellow the cells were plated on coated EZ microscopy slides. The cells were exposed and stained with Lucifer yellow as described above (2.7). After fixation, the cells were then permeabilized and blocked in 5% normal goat serum, PBS, 0.05% saponin for 1 h at room temperature. Then the cells were stained with anti-LAMP-1 (1:50) diluted in antibody staining buffer (1% BSA/PBS, 0.05% saponin) over night at 4°C followed by secondary antibody staining as described for LC3B, and analyzed with confocal microscopy (LSM710, Zeiss).

2.10 DQ red BSA lysosomal activity assay

This assay relies on the cleavage of the self-quenched DQ™ Red BSA protease substrates in an acidic compartment to generate highly fluorescent fragments. The cells were seeded on a 48 well plate or on EZ microscope slide. The staining was done as described in (Marwaha and Sharma 2017). Briefly, DQ red BSA (10 µg/mL) was used in the exposure medium. At the end of exposure, the cells were washed twice in PBS and fixed in 4% PFA for 15 min at room temperature. The cells were washed again with PBS and analyzed for fluorescence with the Spectramax i3x plate reader (Ex590 nm/Em620 nm) plate reader using the well scan function, were 80 different points were read in each well. The total number of cells in each well was counted using the Spectramax i3x plate reader, minimax 300 Imaging Cytometer module. The DQ red BSA fluorescence readout was then normalized to the total number of cells. For microscopic analysis, the EZ microscopy slide were mounted by using ProLong® mounting medium and a coverslip. The images were taken using confocal microscope (LSM710, Zeiss).

2.11 Western blot

HepG2 cells were washed twice in ice cold PBS and placed at -70°C until the next day. The cells were then scraped in lysis buffer containing 0.8% SDS, halt proteinase inhibitor cocktail and phosphatase inhibitor cocktail. The samples were then centrifuged (10 000 x g, 1 min) through a QIAshredder (Qiagen) for homogenization. The protein concentrations were quantified by using Bio-Rad DC protein assay kit. Western blotting was then performed as described in (Solhaug et al. 2012), using the NuPage Novex system from Invitrogen and the following antibodies: LC3B (1:1000), p-mTOR (S2448; 1:1000), p-p70S6K (Thr389; 1:1000), β-Actin Rabbit mAb HRP conjugate (1:4000), and Anti-Rabbit IgG HRP-linked antibody (1:5000) and p62 (1:2000). For the p62 antibody, the anti-guinea pig IRDye680RD (1:5000) (LiCor) was used together with the Odyssey Imaging System.

2.12 Statistical analysis

The data analyses were performed using Sigma Plot version 12.0. Statistical significance ($p < 0.05$) was assessed using 1-way-ANOVA, followed by Dunnett's post-test between control and treated samples or Tukey's post-test between two treated groups.

Methods for cell cycle, mitochondria staining and lipid droplet staining can be found in supplementary, methods.

3. Results

3.1 Treatment with AOD induced cell vacuolization

To assess the effect of AOD on HepG2 cells, the cells were treated with AOD (10 µM) for 3-48 h before investigation by phase contrast imaging. The microscopic pictures in Figure 2A shows that AOD-treatment induced vacuolization starting already after 3-6 h exposure. The vacuoles were multi-sized, and their number and size increased by time. The vacuolization was transient, with a peak between 6-9 h. After 48 h only a few vacuoles were visible. While 10 µM AOD clearly induced considerable vacuolization, both lower (5 µM) as well as higher (20 µM) concentrations of AOD induced only a few vacuoles (data not shown). Transmission electron microscopy revealed that the cytoplasmic vacuoles were translucent and occupy a large part of the cytoplasmic section (Figure 2B). Cellular nuclei were intact with similar appearance as untreated samples. AOD was also found to induce vacuoles, at similar concentrations, in the mouse macrophage cell line, RAW264.7 (supplementary Figure S1) and the human osteosarcoma cell line U2OS (data not shown). Interestingly, treatment with the well-known CerS inhibitor fumonisin B1 had no effect on the vacuolization in AOD treated cells

(supplementary Figure S2), which indicates that the N-acylated metabolites is not the main driver of the vacuolization process.

3.2 High concentrations of AOD induced cell death

The formation of cytoplasmic vacuoles is commonly found in some forms of non-apoptotic cell death, such as necroptosis, paraptosis and methuosis (Cingolani et al. 2017; Shubin et al. 2016). We therefore investigated if the AOD-associated vacuolization were linked to any possible ongoing cell death processes (Figure 3). AOD concentrations up to 10 µM induced no cell death measured as necrosis (CellTox Green) or apoptosis (caspase 3/7 activity), either after 6 h or more prolonged exposure (24 h). However, higher concentrations (15 and 20 µM) of AOD induced both necrosis and apoptosis. Metabolic activity/proliferation (Alamar Blue) was also reduced at cytotoxic concentrations, thus reflecting the induction of cell death. In agreement with this, concentrations of AOD up to 10 µM had no or only minor effects on the relative distribution of cells in the cell cycle, suggesting that this process was not affected (supplementary Figure S3). Furthermore, the receptor-interacting serine/threonine-protein kinase 1 (RIPK1) inhibitor, necrostatin-1, an inhibitor of necroptosis, had no obvious effect on AOD-induced vacuolization (supplementary Figure S4). Paraptosis is associated with cytoplasmic vacuolization by endoplasmic reticulum and mitochondrial swelling in addition to accumulation of lipid droplets. To explore the possibility of AOD-induced paraptosis, the mitochondria were stained with mitotracker red and observed with fluorescence microscopy. However, there were no differences in the mitochondrial morphology between control and cells treated with 10 µM AOD (supplementary Figure S5). Furthermore, the AOD-induced vacuoles were not stained by the lipid droplet marker, Oil Red O (supplementary Figure S6), thus ruling out the possibility that the AOD-induced vacuoles were lipid droplets. In summary, AOD treatment results in vacuolization that are not linked to cell death processes.

3.3 Treatment with AOD affected vesicular transport systems

The proteomic analysis (Table 1) revealed the possibility that 5 µM AOD affected proteins in the phagosome-, ErbB-, gap-junction- and HIF-1 signaling pathways as well as carbohydrate metabolism; at 10 µM the pathway identifier for the vesicle-mediated transport from golgi to the plasma membrane was changed. Overall, the results suggested that effects on various parts of the vesicular transport system might be involved in the induced vacuolization.

Vesicular transport starts at the plasma membrane. Thus, we next explored possible effects of AOD on the plasma membrane by staining their lipid microdomains (also called lipid rafts) with cholera toxin subunit B (CT-B) conjugated to Alexa Fluor 488. As analyzed by fluorescence microscopy, AOD caused a more intense staining (Figure 4), suggesting that AOD induced a clustering or change of these lipid microdomains. As lipid microdomains are involved in endocytosis, we explored if AOD modified the uptake of Lucifer yellow, a fluid-phase tracer often used when studying macropinocytosis (Shubin et al. 2016). As illustrated in Figure 5A and quantified by plate reader (Figure 5B), AOD exposure only slightly increased the uptake of Lucifer yellow. It should also be noted that the large vacuoles were apparently not filled with Lucifer yellow (Figure 5 and 6).

To further explore the identity of the AOD-induced vacuoles, we stained for lysosomal-associated membrane protein-1 (LAMP-1), a glycoprotein abundantly expressed on late endosomes and lysosomes. Indeed, the AOD-induced vacuoles were LAMP-1 positive (Figure 6). Treatment with AOD also induced a marked increase in lysotracker red staining, which is a marker of acidic organelles (Figure 7AB). Both the LAMP-1- and lysotracker red positive structures were somewhat larger in AOD treated cells. Together these data suggest that AOD-induced vacuoles are swollen late endosomes or lysosomes. Interestingly, the largest vacuoles were not positive for lysotracker red staining (Figure 7A), suggesting that these swollen vacuoles are no longer acidic.

As AOD seemed to cause an enlargement of late endosomes /lysosomes, we tested if the AOD-induced vacuolization was dependent of acid lysosomes by the addition of chloroquine or concanamycin A, which increase the lysosomal pH. Interestingly, both compounds reduced the AOD-induced vacuolization to control level (Figure 8), strongly suggesting that the AOD-induced vacuolization is dependent of acidic lysosomes.

3.5 Treatment with AOD reduced lysosomal degradation capacity

Since AOD treatment led to enlargement of late endosomes or lysosomes, it was of interest to see whether the function of the endolysosomal degradation pathway was compromised. Lysosomal degradation activity was assessed by measuring the cleavage of the model cargo DQ™ Red BSA, which is a self-quenched protease substrate turned into fluorescent fragments upon cleavage. Thus, the red fluorescent puncta seen in control cells reflect the lysosomal degradation of DQ-BSA (Figure 9A). Interestingly, in AOD-treated cells the degradation of DQ-BSA was reduced by ~30%. For comparison, cells treated with the lysosomal inhibitor concanamycin A, which increases lysosomal pH by inhibiting the lysosomal v-ATPase, demonstrated a 50% reduction in DQ-BSA degradation (Figure 9B).

Since treatment with AOD seems to reduce endosomal protein degradation capacity, it was of interest to see whether AOD would also alter autophagic degradation activity as both pathways require functional lysosomes. To this end we looked for changes in the levels of the autophagosomal protein LC3B, which is degraded in the lysosomes along with the autophagic cargo and considered a marker for autophagosome number (Klionsky et al. 2016). Following treatment with AOD, the level of LC3B was clearly increased, as determined by immunofluorescence staining of LC3B (Figure 10A) and western blotting (Figure 10BC).

However, as accumulation of autophagosomes may be a result of both autophagic activation or a blockage of autophagic degradation (Klionsky et al. 2016), we had to

discriminate between these two scenarios by using the lysosomal inhibitor chloroquine that inhibits autophagic degradation in the lysosomes (Klionsky et al. 2016). When the cells were treated with either chloroquine alone or chloroquine in combination with AOD, there was no difference in the accumulation of LC3 (Figure 11), suggesting that AOD treatment does not induce generation of new autophagosomes, but rather seem to block the degradation. Moreover, as seen in Figure 10BC, AOD also markedly increased the level of p62, another well-known autophagosomal marker that is degraded during autophagy (Klionsky et al. 2016). In contrast, AOD treatment did not affect the activity of mTORC1, the main regulator of autophagy (Klionsky et al. 2016). Neither the phosphorylation of mTOR itself, nor the downstream target S6K was reduced by AOD (Figure 10BC). As expected, rapamycin, an inhibitor of mTOR and thus a positive control for autophagy induction, completely abolished phosphorylation of mTOR and S6K (supplementary Figure S7). Together, these data support our hypothesis that AOD do not enhance the rate of autophagosome formation, but rather reduce autolysosomal degradation (autophagic flux).

Cytoplasmatic vacuolization induced by several toxins is found to be inhibited by the v-ATPase inhibitor bafilomycin A1, thus indicate the importance of lysosomal pH in this process (Shubin et al. 2016). Furthermore, as reduced autolysosomal degradation can be caused by an increased lysosomal pH (Klionsky et al. 2016), we investigated the impact of AOD on lysosome pH. However, the lysosomal pH sensor Yellow/Blue DND-160 (supplementary Figure S8), revealed that AOD rather led to an overall decrease of lysosomal pH (Figure 12), although the largest vacuoles were not positive for lysotracker red staining (Figure 7).

4. Discussion

Here we report that AOD induced a transient massive accumulation of vacuoles in HepG2 cells. The vacuolization was seen at non-cytotoxic concentrations and not linked to cell death processes. Proteomic analyses indicated that vesicular transport may be a target for AOD, and

further studies suggested that the vacuoles originated from a disorder of the late stages of the endolysosomal pathway.

AOD did not increase the level of sphinganine in treated cells (Uhlig et al. 2008), suggesting that AOD has no major impact on CerS. Furthermore, the CerS inhibitor and sphingosine analogue fumonisin B1 did not cause any vacuolization itself nor reduce the AOD-induced vacuolization. Thus, the vacuolization is apparently not directly linked to sphingosine and/or any possible N-acylated AOD metabolites. Interestingly, also the natural sphingolipid and CerS inhibitor Jaspine B, is found to induce vacuolization independent of its action on the sphingolipid metabolism (Cingolani et al. 2017).

Cytoplasmic vacuolization in mammalian cells can be irreversible or transient. Inducers of irreversible vacuolization causes known types of caspase-independent cell death including necroptosis, methuosis, paraptosis and paraptosis-like cell death (Shubin et al. 2016). Irreversible vacuolization marks cytopathological conditions leading to cell death, as long as the cytotoxic stimulus is present. Here however, we observe that the vacuolization was transient and occurring at non-cytotoxic conditions, while higher cytotoxic concentration of AOD induced only a few vacuoles. Use of specific inhibitors, check of metabolic activity and microscopic evaluations revealed that the vacuolization was incompatible with the different forms of caspase-independent cell death processes associated with vacuolization. Thus, our results are in agreement with previous studies that conclude that transient vacuolization is most often not associated with cell death (Shubin et al. 2016).

Lipophilic chemicals will accumulate in cellular membranes. This may change the membrane properties, and several studies have revealed that this may result in transient vacuolization (Young et al. 2019; Young et al. 2016), as here seen for AOD. Transient vacuolization might be due increased formation or reduced processing of vacuoles involved in endocytosis, autophagy or by swelling of lysosomes (Choy et al. 2018; Schulze et al. 2017;

Shubin et al. 2016). The proteomic analysis (Table 1) showing that AOD affect the level of several proteins involved in the phagosome pathways; support the hypothesis that AOD may affect various parts of the vesicular transport systems. Sphingolipids are essential components for a proper function of lipid microdomain, both with regard to cell signalling as well as certain types of endocytosis (Bieberich 2018). More specifically, the sphingosine analogue, and sphingosine 1 kinase inhibitor SK1-I, are suggested to enter the cells by cholesterol-dependent endocytosis associated to lipid microdomain (Young et al. 2016). Both disruption as well as clustering of microdomain areas have been found to interfere with endocytosis (Ewers and Helenius 2011; Rodal et al. 1999). Here we found that AOD resulted in an aggregation of lipid microdomain areas as seen as a more intense staining of the fluorescence coupled microdomain probe cholera toxin subunit B. Thus, indicating that AOD accumulate in lipid membranes and possibly enter the cells via lipid-microdomain mediated endocytosis.

Increased vacuolization may be due to increased formation of vesicles by endocytosis as well as autophagy. Interestingly, Jaspine B-induced vacuolization was linked to enhanced macropinocytosis (Cingolani et al. 2017), a regulated form of endocytosis that mediates the non-selective uptake of solute molecules including nutrients and antigens (Swanson 2008). The AOD-increased macropinocytosis was, however, too low to account for the massive increase in vacuoles observed, and the vacuoles did not contain the macropinocytic cargo Lucifer yellow. Furthermore, autophagy was not increased as judged by an unchanged activity of the mTOR pathway and a reduced autophagic flux. However, as the AOD-induced vacuoles were LAMP-1 positive, they most likely originate from late endosomes or lysosomes (Cheng et al. 2018).

Vacuolization may occur by a mechanism referred to as lysosomal trapping. In this process, lipophilic and amphiphilic drugs with ionizable amines (pKa > 8-10) accumulate in lysosomes and thereby increasing the intraorganellar osmotic pressure. The equilibration of osmotic pressure by water diffusion across the organelle membranes leads to the formation of

vacuoles (Marceau et al. 2012). This might be a possible mechanism for AOD-induced vacuolization. As AOD most probably due to its fatty acid unit, accumulate in the plasmamembrane, AOD will likely enter the cells by endocytosis thereby ending up with its amine group facing the lumen of the lysosome, which in an acid environment will turn positive. Interestingly, inhibition of the v-ATPase with concanamycin A, or incubation with chloroquine, which make the lysosomes basic, completely blocked the AOD-induced vacuolization indicating that the vacuolization is dependent of acidic lysosomes. Similarly, bafilomycin A1 has been found to inhibit vacuolization induced by a number of well-known lysosomal trapping compounds (Marceau et al. 2012; Schulze et al. 2017; Shubin et al. 2016). Furthermore, these type of compounds will also reduce lysosomal degradation capacity (Seglen and Gordon 1980) as here seen following AOD exposure. Moreover, lysosomal trapping agents are known to block autophagic degradation (Parks and Marceau 2016; Solitro and MacKeigan 2016). Altogether, lysosomal trapping is a likely mechanism of AOD-induced vacuolization that are worth further testing.

However, other mechanisms for vacuolization of the endosomal/lysosomal organelles with several similarities with AOD-induced vacuolization have been described and should not be excluded. Sphingosine kinase 1 is recently found to cooperate with autophagy to maintain endocytic membrane trafficking (Young et al. 2016). Here, several, sphingosine kinase 1 inhibitors, independent of their kinase activity, including FTY720, as well as sphingosine itself induce transient vacuolization by promoting membrane fusion. Their results had great similarities to our findings; the vacuoles were of late endosomal/lysosomal origin, failed to accumulate the acidic probe lysotracker red and analysis of LC3B and p62 revealed that the autophagic flux was blocked. Furthermore, sphingosine is involved in the pathophysiology of Nieman-Pick disease C. Here sphingosine, alongside with other lipids accumulate in lysosomes because of mutations in the lysosomal proteins NCP1/2. As a consequence, calcium release

from the lysosomes is blocked (Hoglinger et al. 2015). Regulation of the calcium release from the lysosomes to the cytoplasm is associated with both lysosomal regeneration (Cao et al. 2017) and autophagy (Medina et al. 2015). The lysosomal calcium release channel transient receptor potential mucolipin 1 (TRPML1) is found to be a regulator of lysosome size, by controlling both lysosome biogenesis and reformation (Cao et al. 2017). Thus, we cannot totally exclude the possibility that other mechanisms besides lysosomal trapping are involved in AOD-induced vacuolization.

The nonfunctional lysosomes and reduced clearance of vacuole/reformation of lysosomes is in accordance with the observation that lysotracker red failed to accumulate in the big vacuoles. It is well-known that lysosomal stress increases transcription of genes associated to lysosomes and autophagy in order to restore the lysosomal capacity (Palmieri et al. 2011; Sardiello et al. 2009). As lysosomal protein degradation is reduced, the overall lysosomal acidification observed in AOD-treated cells may rather be a result of this type of compensatory increase in lysosomal biogenesis. Thus, over time the increased biogenesis of lysosomes seems to restore the lysosomal balance. Accordingly, the clearance of the vacuoles induced by sphingosine kinase 1 was found to be dependent on CerS, lysosomal biogenesis and restoration of autophagic flux (Young et al. 2016). An explanation to the transient part of the vacuolization process might be lysosomal exocytosis shedding of vesicles, as observed in the case of the sphingosine analogue FTY720 (Young et al. 2019); possibly combined with AOD metabolism. Thus, further studies should include examination of extracellular vesicles as well as AOD metabolism.

In conclusion, AOD induced a transient increased vacuolization originating from disturbances of the endolysosomal pathway, thereby reducing the endosomal degradation capacity.

Conflicts of interest:

The authors declare that there are no conflicts of interest

Acknowledgements

The authors wish to thank FUNtox, strategic initiative of the Norwegian Veterinary Institute for funding. Maria L Torgersen was funded by the Norwegian Research Council grant nr. 274574. We also wish to thank Silvio Uhlig, Alfred H. Merrill and Roland T. Riley for valuable discussion of the chemical properties of AOD. The authors also thank the Imaging Centre at the Norwegian University of life Sciences (NMBU) for the use of transmission electron microscope.

Referenses:

Bieberich, E. Sphingolipids and lipid rafts: Novel concepts and methods of analysis. Chem Phys Lipids 2018;216:114-131

Blank, N.; Schiller, M., et al. Cholera toxin binds to lipid rafts but has a limited specificity for ganglioside GM1. Immunol Cell Biol 2007;85:378-382

Breiden, B.; Sandhoff, K. Emerging mechanisms of drug-induced phospholipidosis. Biol Chem 2019;

Cao, Q.; Yang, Y., et al. The lysosomal Ca(2+) release channel TRPML1 regulates lysosome size by activating calmodulin. The Journal of biological chemistry 2017;292:8424-8435

Cecconi, F.; Piacentini, M., et al. The involvement of cell death and survival in neural tube defects: a distinct role for apoptosis and autophagy? Cell death and differentiation 2008;15:1170-1177

Cheng, X.T.; Xie, Y.X., et al. Characterization of LAMP1-labeled nondegradative lysosomal and endocytic compartments in neurons. J Cell Biol 2018;217:3127-3139

Chiricozzi, E.; Loberto, N., et al. Sphingolipids role in the regulation of inflammatory response: From leukocyte biology to bacterial infection. Journal of leukocyte biology 2018;103:445-456

Choy, C.H.; Saffi, G., et al. Lysosome enlargement during inhibition of the lipid kinase PIKfyve proceeds through lysosome coalescence. J Cell Sci 2018;131

Cingolani, F.; Simbari, F., et al. Jaspine B induces nonapoptotic cell death in gastric cancer cells independently of its inhibition of ceramide synthase. Journal of Lipid Research 2017;58:1500-1513

Coffey, E.E.; Beckel, J.M., et al. Lysosomal alkalization and dysfunction in human fibroblasts with the Alzheimer's disease-linked presenilin 1 A246E mutation can be reversed with cAMP. Neuroscience 2014;263:111-124

Ewers, H.; Helenius, A. Lipid-mediated endocytosis. Cold Spring Harb Perspect Biol 2011;3:a004721

Grassi, S.; Chiricozzi, E., et al. Sphingolipids and neuronal degeneration in lysosomal storage disorders. J Neurochem 2019;148:600-611

Grootaert, M.O.J.; Roth, L., et al. Defective Autophagy in Atherosclerosis: To Die or to Senesce? Oxid Med Cell Longev 2018;2018:7687083

Guo, X.; Dong, Y., et al. Patulin induces pro-survival functions via autophagy inhibition and p62 accumulation. Cell Death Dis 2013;4:e822

Hait, N.C.; Maiti, A. The Role of Sphingosine-1-Phosphate and Ceramide-1-Phosphate in Inflammation and Cancer. Mediators Inflamm 2017;2017:4806541

Hoglinger, D.; Haberkant, P., et al. Intracellular sphingosine releases calcium from lysosomes. Elife 2015;4

Hornemann, T.; Worgall, T.S. Sphingolipids and atherosclerosis. Atherosclerosis 2013;226:16-28

Inpanathan, S.; Botelho, R.J. The Lysosome Signaling Platform: Adapting With the Times. Front Cell Dev Biol 2019;7:113

Ivanova, L.; Uhlig, S. A bioassay for the simultaneous measurement of metabolic activity, membrane integrity, and lysosomal activity in cell cultures. AnalBiochem 2008;379:16-19

Kitatani, K.; Idkowiak-Baldys, J., et al. The sphingolipid salvage pathway in ceramide metabolism and signaling. Cellular Signalling 2008;20:1010-1018

Klionsky, D.J.; Abdelmohsen, K., et al. Guidelines for the use and interpretation of assays for monitoring autophagy (3rd edition). Autophagy 2016;12:1-222

Kroemer, G.; Marino, G., et al. Autophagy and the integrated stress response. MolCell 2010;40:280-293

Lai, M.; La Rocca, V., et al. Sphingolipid/Ceramide Pathways and Autophagy in the Onset and Progression of Melanoma: Novel Therapeutic Targets and Opportunities. International journal of molecular sciences 2019;20

Lai, M.K.; Chew, W.S., et al. Biological Effects of Naturally Occurring Sphingolipids, Uncommon Variants, and Their Analogs. Neuromolecular Med 2016;18:396-414

Marasas, W.F.; Riley, R.T., et al. Fumonisins disrupt sphingolipid metabolism, folate transport, and neural tube development in embryo culture and in vivo: a potential risk factor for human

neural tube defects among populations consuming fumonisin-contaminated maize. J Nutr 2004;134:711-716
Maresca. From Gut to the brain: Journey and Pathophysiological Effects of the Food-Associated Trichothecent Mycotoxin deoxynivalenol. Toxins 2013; 5(4):784-820.
Marceau, F.; Bawolak, M.T., et al. Cation trapping by cellular acidic compartments: beyond the concept of lysosomotropic drugs. Toxicol Appl Pharmacol 2012;259:1-12
Martens, S.; Nakamura, S., et al. Phospholipids in Autophagosome Formation and Fusion. J Mol Biol 2016;
Marwaha, R.; Sharma, M. DQ-Red BSA Trafficking Assay in Cultured Cells to Assess Cargo Delivery to Lysosomes. Bio Protoc 2017;7
Medina, D.L.; Di Paola, S., et al. Lysosomal calcium signalling regulates autophagy through calcineurin and TFEB. Nat Cell Biol 2015;17:288-299
Palmieri, M.; Impey, S., et al. Characterization of the CLEAR network reveals an integrated control of cellular clearance pathways. Hum Mol Genet 2011;20:3852-3866
Parks, A.; Marceau, F. Lysosomotropic cationic drugs induce cytostatic and cytotoxic effects: Role of liposolubility and autophagic flux and antagonism by cholesterol ablation. Toxicol Appl Pharmacol 2016;305:55-65
Pujol-Lereis, L.M. Alteration of Sphingolipids in Biofluids: Implications for Neurodegenerative Diseases. International journal of molecular sciences 2019;20
Riley, R.T.; Merrill, A.H., Jr. Ceramide synthase inhibition by fumonisins: a perfect storm of perturbed sphingolipid metabolism, signaling, and disease. J Lipid Res 2019;60:1183-1189
Rodal, S.K.; Skretting, G., et al. Extraction of cholesterol with methyl-beta-cyclodextrin perturbs formation of clathrin-coated endocytic vesicles. Mol Biol Cell 1999;10:961-974
Sardiello, M.; Palmieri, M., et al. A gene network regulating lysosomal biogenesis and function. Science 2009;325:473-477
Schulze, U.; Vollenbroker, B., et al. Cellular vacuolization caused by overexpression of the PIKfyve-binding deficient Vac14(L156R) is rescued by starvation and inhibition of vacuolar-ATPase. Biochim Biophys Acta Mol Cell Res 2017;1864:749-759
Seglen, P.O.; Gordon, P.B. Effects of lysosomotropic monoamines, diamines, amino alcohols, and other amino compounds on protein degradation and protein synthesis in isolated rat hepatocytes. Mol Pharmacol 1980;18:468-475
Shubin, A.V.; Demidyuk, I.V., et al. Cytoplasmic vacuolization in cell death and survival. Oncotarget 2016;7:55863-55889
Solhaug, A.; Karlsoen, L.M., et al. Immunomodulatory effects of individual and combined mycotoxins in the THP-1 cell line. Toxicology in vitro : an international journal published in association with BIBRA 2016;36:120-132
Solhaug, A.; Torgersen, M.L., et al. Autophagy and senescence, stress responses induced by the DNA-damaging mycotoxin alternariol. Toxicology 2014;326:119-129
Solhaug, A.; Vines, L.L., et al. Mechanisms involved in alternariol-induced cell cycle arrest. Mutation research 2012;738-739:1-11
Solitro, A.R.; MacKeigan, J.P. Leaving the lysosome behind: novel developments in autophagy inhibition. Future Med Chem 2016;8:73-86
Swanson, J.A. Shaping cups into phagosomes and macropinosomes. Nat Rev Mol Cell Biol 2008;9:639-649
Thelen, A.M.; Zoncu, R. Emerging Roles for the Lysosome in Lipid Metabolism. Trends in cell biology 2017;27:833-850
Uhlig, S.; Eriksen, G.S., et al. Faces of a changing climate: semi-quantitative multi-mycotoxin analysis of grain grown in exceptional climatic conditions in norway. Toxins 2013;5:1682-1697
Uhlig, S.; Ivanova, L., et al. 2-Amino-14,16-dimethyloctadecan-3-ol: *in vitro* bioactivity and bio-production by the fungus Fusarium avenaceum. World Mycotoxin Journal 2008;1:49-58
Uhlig, S.; Petersen, D., et al. 2-Amino-14,16-dimethyloctadecan-3-ol, a new sphingosine analogue toxin in the fungal genus Fusarium. Toxicon 2005;46:513-522

van Echten-Deckert, G.; Alam, S. Sphingolipid metabolism - an ambiguous regulator of autophagy in the brain. Biol Chem 2018;399:837-850

Wang, Y.; Zheng, W., et al. Zearalenone induces apoptosis and cytoprotective autophagy in primary Leydig cells. Toxicology Letters 2014;226:182-191

Young, M.M.; Bui, V., et al. FTY720 induces non-canonical phosphatidylserine externalization and cell death in acute myeloid leukemia. Cell Death Dis 2019;10:847

Young, M.M.; Kester, M., et al. Sphingolipids: regulators of crosstalk between apoptosis and autophagy. J Lipid Res 2013;54:5-19

Young, M.M.; Takahashi, Y., et al. Sphingosine Kinase 1 Cooperates with Autophagy to Maintain Endocytic Membrane Trafficking. Cell Rep 2016;17:1532-1545

Zitomer, N.C.; Mitchell, T., et al. Ceramide Synthase Inhibition by Fumonisin B-1 Causes Accumulation of 1-Deoxysphinganine a novel category of bioactive 1-deoxysphingoid bases and 1-deoxydihydroceramides biosynthesized by mammalian cell lines and animals. J Biol Chem 2009;284:4786-4795

Figure legends:

Figure 1: Molecular structures of AOD, sphinganine, sphingosine and fumonisin B1.

Figure 2: AOD induces vacuolization of HepG2 cells. Cells were treated with AOD (10 µM) and examined using (A) light microscopy for the indicated time points (scale bar = 50 µm) or (B) transmission electronic microscopy after 6 h exposure (scale bar = 2 µm).

Figure 3: AOD induces cell death in HepG2 cells. Cells were treated with AOD (5-20 µM) for indicated time points and analyzed for necrotic cells by the Celltox Green assay (A). AOD 20 µM (24 h) is comparable to positive control and caused 100% cell death (not shown). n=5, for apoptotic cells; caspase 3/7 activity, n=3 (B) or metabolic activity by the Alamar Blue assay (C). The data represent mean ± SEM of 3-5 independent experiments. * indicates significantly different from control (1-way ANOVA with Dunnett post-test).

Figure 4: AOD-treatment change the appearance of lipid microdomains. Cells were treated with AOD (10 µM) for 6 h, fixed and prepared for immunofluorescence staining of lipid microdomains (cholera toxin subunit B, green) and DAPI staining of nuclei (blue) and analyzed by confocal microscopy. Representative images are shown. Scale bar = 20 µm.

Figure 5: AOD induces macropinocytosis. Cells were treated with AOD (10 µM, 6 h) and analyzed for macropinocytosis by uptake of Lucifer yellow. The cells were fixed and analyzed by confocal microscopy (A, Scale bar = 20 µm.) and plate reader (B). The data are quantified and represent mean ± SEM of 3 independent experiments. * indicates significantly different from control (1-way ANOVA with Dunnett`s post test).

Figure 6: AOD-induced vacuoles are of late endosomal or lysosomal origin. Cells were treated with AOD (10 µM, 6 h) and analyzed for macropinocytosis by Lucifer yellow (yellow) uptake, fixed and stained with the late endosome or lysosomal marker LAMP-1 (red). The cells were then visualized by confocal microscopy. Representative images are shown. Scale bar = 20 µm.

Figure 7: AOD induces increased level of late endosomes or lysosomes. The cells were treated with AOD (10 µM, 6 h), stained with LTR (red) and analyzed by confocal microscopy (A). The nuclei were visualized by DAPI staining (blue) and the cell surface (grey) was visualized by DIC microscopy. Scale bar = 20 µm. The LTR staining was quantified by plate reader (B). The plate reader results represent mean ± SEM of 3 independent experiments. * indicates significantly different from control (student t test).

Figure 8: Lysosome alkalization drugs inhibits AOD induced vacuolization. The cells were treated with AOD (10 µM, 6 h) with or without CQ (5 µM) and Con A (50 nM). Vacuolization was visualized by light microscopy. The pictures are representative of 3 independent experiments. Scale bar = 50 µm.

Figure 9: AOD and lysosomal degradation analyzed by DQ-BSA. The cells were treated with AOD (10 µM, 6 h) and analyzed for DQ-BSA fluorescence by confocal microscopy (A, Scale bar = 20 µm.) or plate reader (B). Concanamycin A (Con A, 50 nM), a v-ATPase inhibitor, was used as positive control. The microscopic images are representative of three independent

experiments. The plate reader results are quantified, and the data represent mean ± SEM of 3-5 independent experiments. * indicates significantly different from control (1-way ANOVA with Dunnett`s post test).

Figure 10: Protein expressions related to macroautophagy. Cells were treated with AOD (5-10 µM) for 6 h and analyzed for LC3B by immunofluorescence (A) and LC3B, p62, P-mTOR (S2448), P-S6K (Thr389) and β-actin by Western blot (B). The western blot results are quantified and normalized to total protein (β-actin). The data represent mean ± SE of 3-5 independent experiments (C). * indicates significantly different from control (1-way ANOVA with Dunnett`s post-test).

Figure 11: AOD and autophagic activity analyzed by LC3B and chloroquine (CQ). Cells were treated with AOD (5 and 10 µM) alone or in combination with CQ (5µM) for 6 h and analyzed by western blotting. The results are quantified and normalized to total protein (β-actin). The data represent mean ± SE of 5 independent experiments (C). Statistical analyses were done by comparing CQ with AOD in combination with CQ (1-way ANOVA with Tukey`s post test).

Figure 12: AOD induces acidification of the lysosomes. Lysosomal pH was investigated by using the lysosensor DND-160, and analyzed by the plate reader. The data are quantified and represent mean ± SEM of 4 independent experiments. * indicates significantly different from control (1-way ANOVA with Dunnett`s post test).

Table 1: Cellular signalling pathways affected in HepG2 cells exposed to AOD (5 and 10 µM) for 6 h.

Table 1: Cellular signalling pathways affected in HepG2 cells exposed to AOD (5 and 10 µM) for 6 h.

Pathway name	Pathway identifier	No of affected proteins	AOD (µM)	Comments
Phagosome pathway	KEGG	4	5	
ErbB signalling pathway	KEGG	3	5	All kinases, incl MAPK1, p21 activated kinase 2
Gap-junction pathway	KEGG	3 TUBa, TUBB, MAPK1	5	Some also included in phagosome pathway
HIF-1 signalling pathway	KEGG	3 CAMK2D, MAPK1, PDHB	5	
Carbohydrate metabolism	KEGG	3 GPT2, PHGDH, PDHB	5	
vesicle-mediated transport from Golgi-to the plasma membrane	Panther Pathway/ reactome		10	
Ubiquitin-proteasome pathway	Panther Pathway/ reactome	5	10	
Expression of proteins related to cytoskeleton and microtubule	All analysis			

AOD

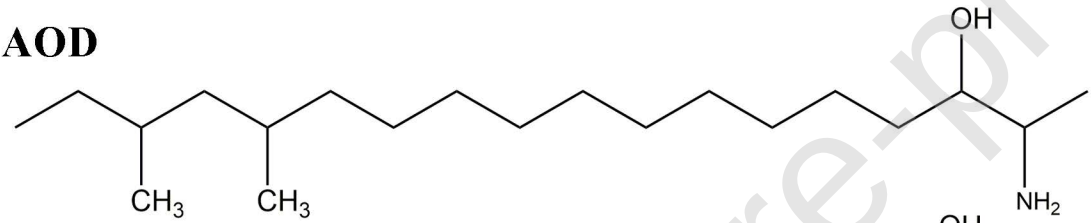

sphinganine

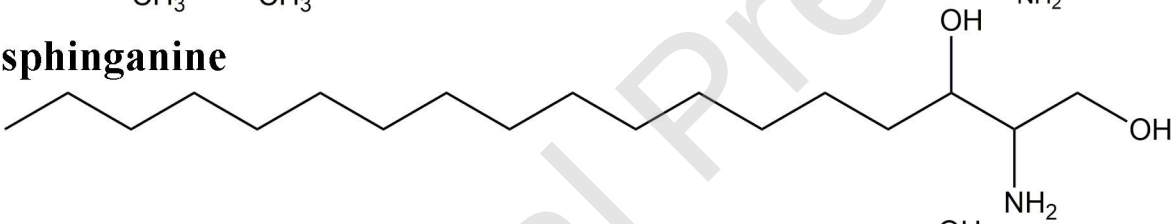

sphingosine

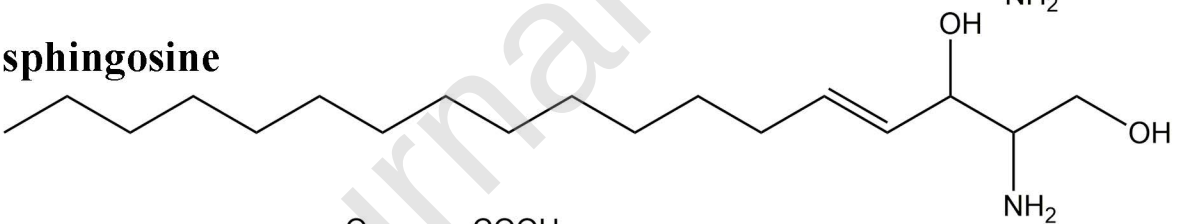

fumonisin B1

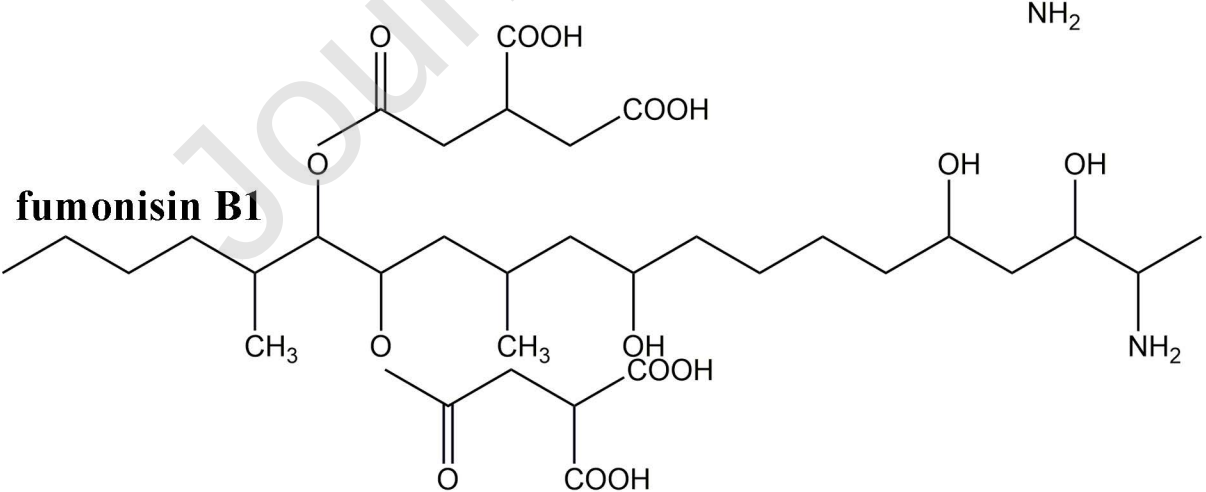

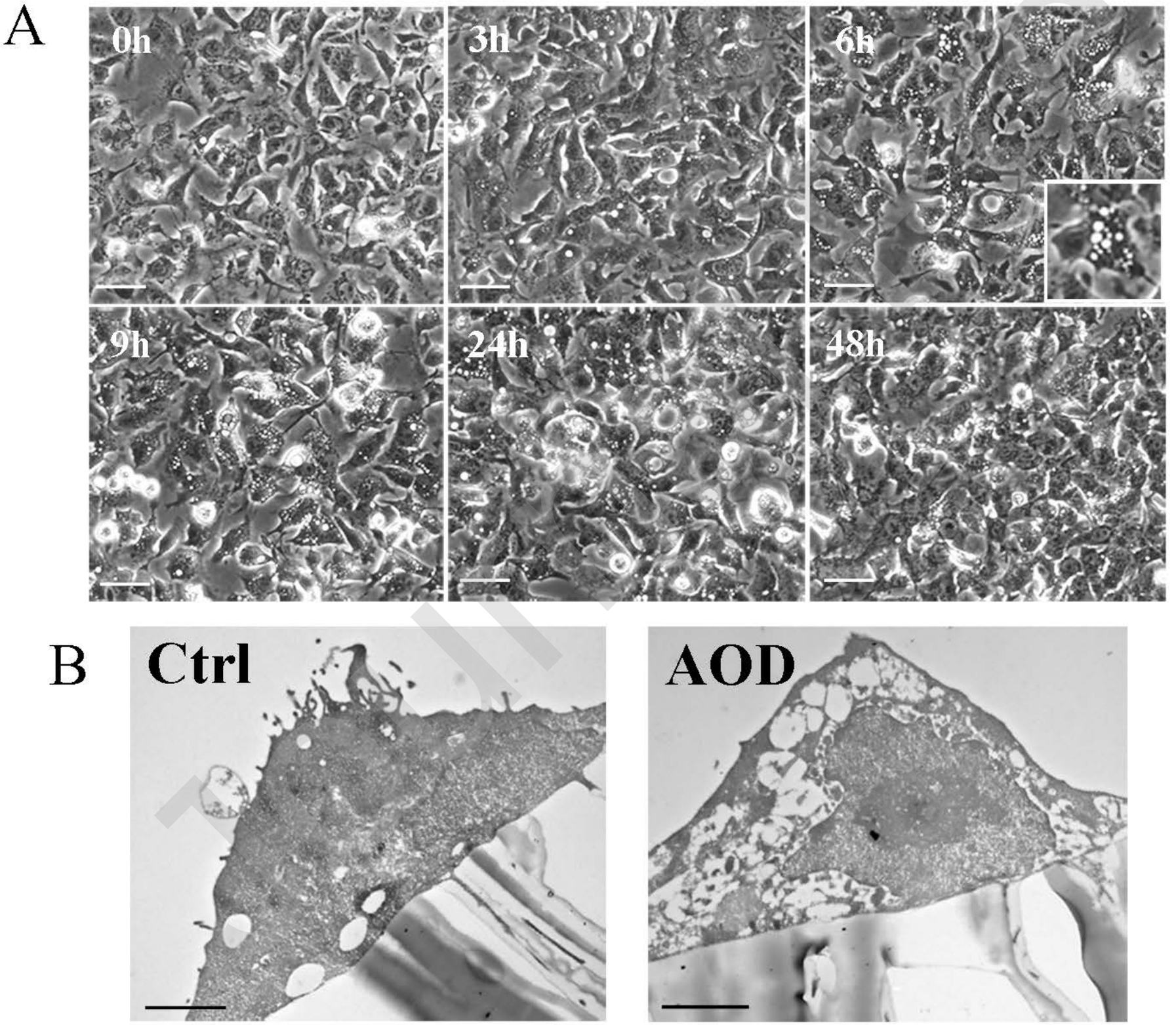
A
0h
3h
6h
9h
24h
48h
B
Ctrl
AOD

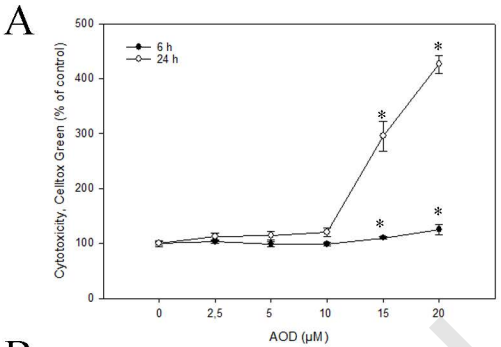
A
6 h
24 h
Cytotoxicity, Celltox Green (% of control)
500
400
300
200
100
0
0
2,5
5
10
15
20
AOD (µM)
*

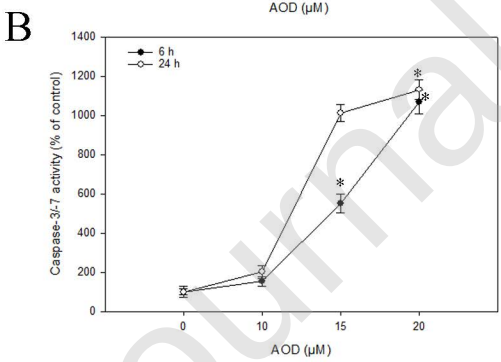
B
6 h
24 h
Caspase-3/7 activity (% of control)
1400
1200
1000
800
600
400
200
0
0
10
15
20
AOD (µM)
*

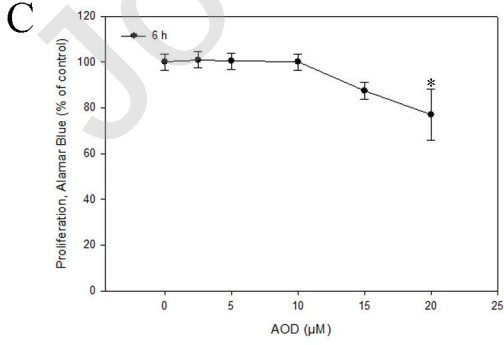
C
6 h
Proliferation, Alamar Blue (% of control)
120
100
80
60
40
20
0
0
5
10
15
20
25
AOD (µM)
*

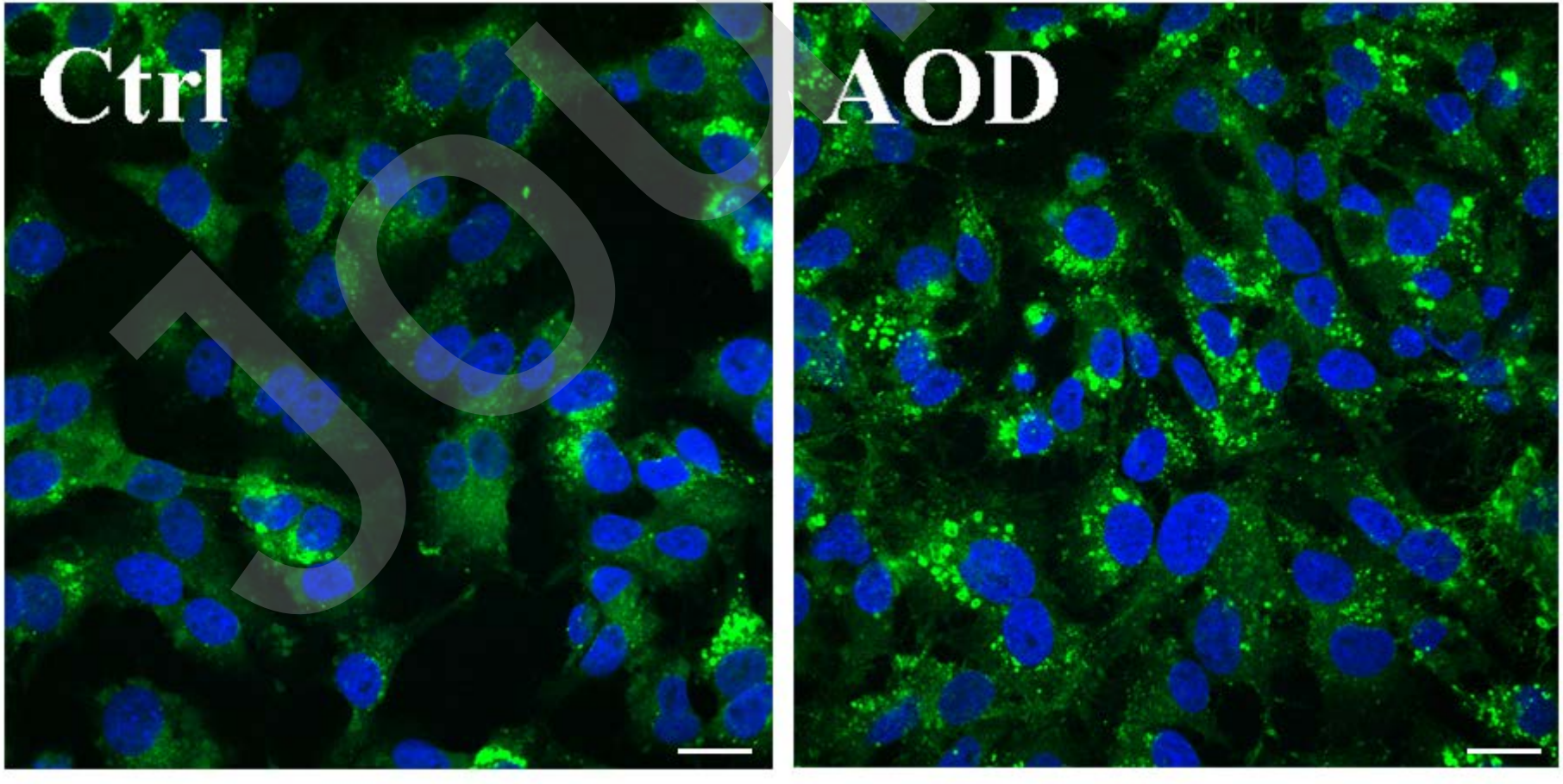
Ctrl
AOD

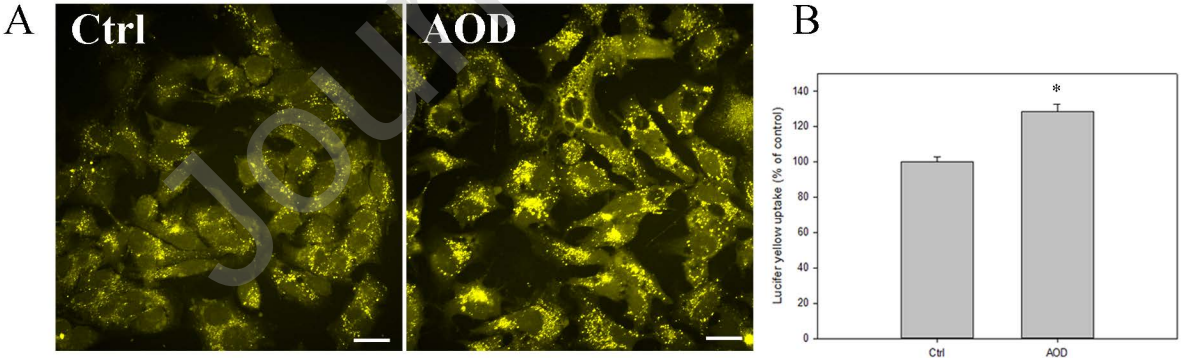
A
Ctrl
AOD
B
Lucifer yellow uptake (% of control)
0
20
40
60
80
100
120
140
*
Ctrl
AOD

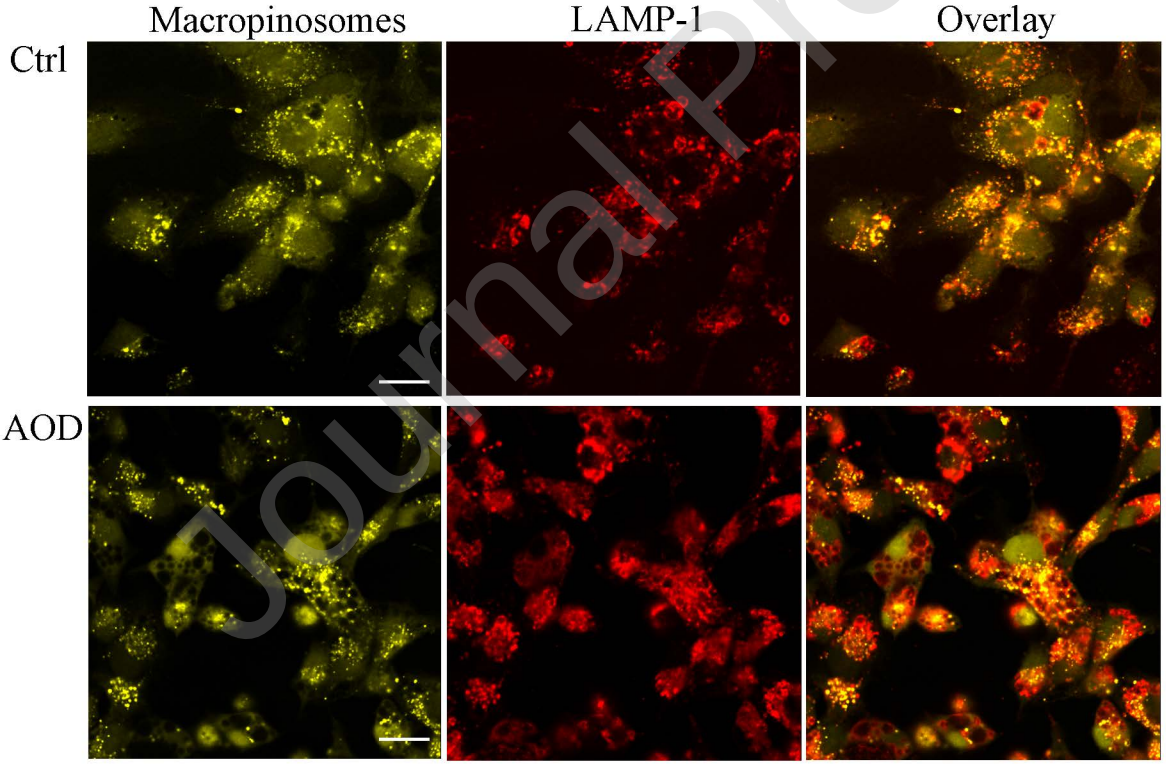
Macropinosomes
LAMP-1
Overlay
Ctrl
AOD

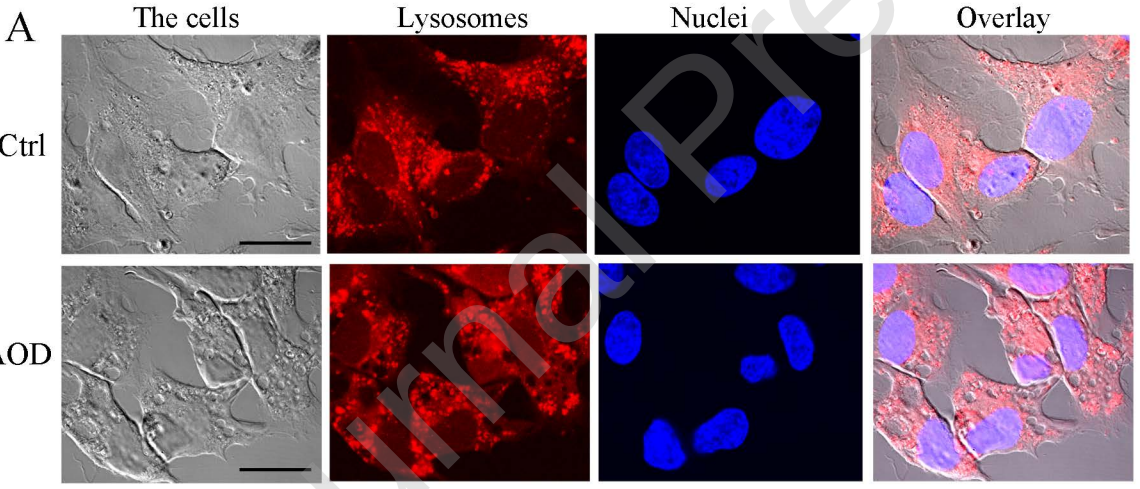
A
The cells
Lysosomes
Nuclei
Overlay
Ctrl
AOD

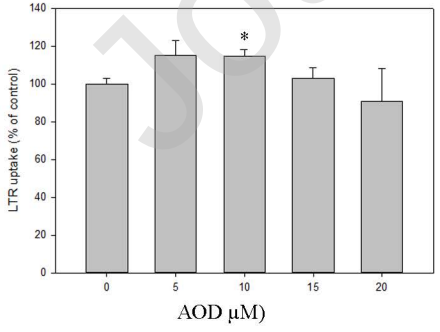
B
LTR uptake (% of control)
140
120
100
80
60
40
20
0
*
0
5
10
15
20
AOD μM)

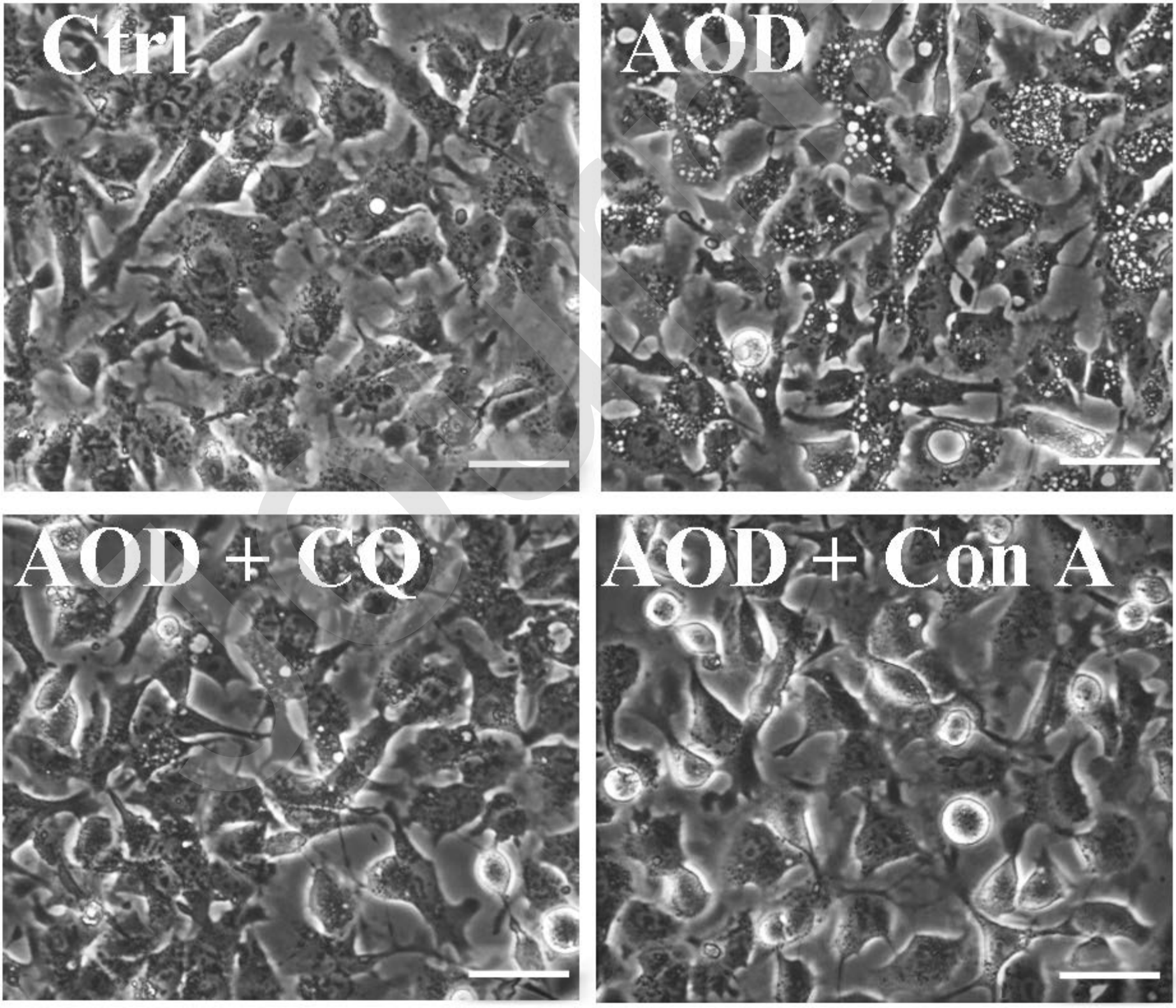
Ctrl
AOD
AOD + CQ
AOD + Con A

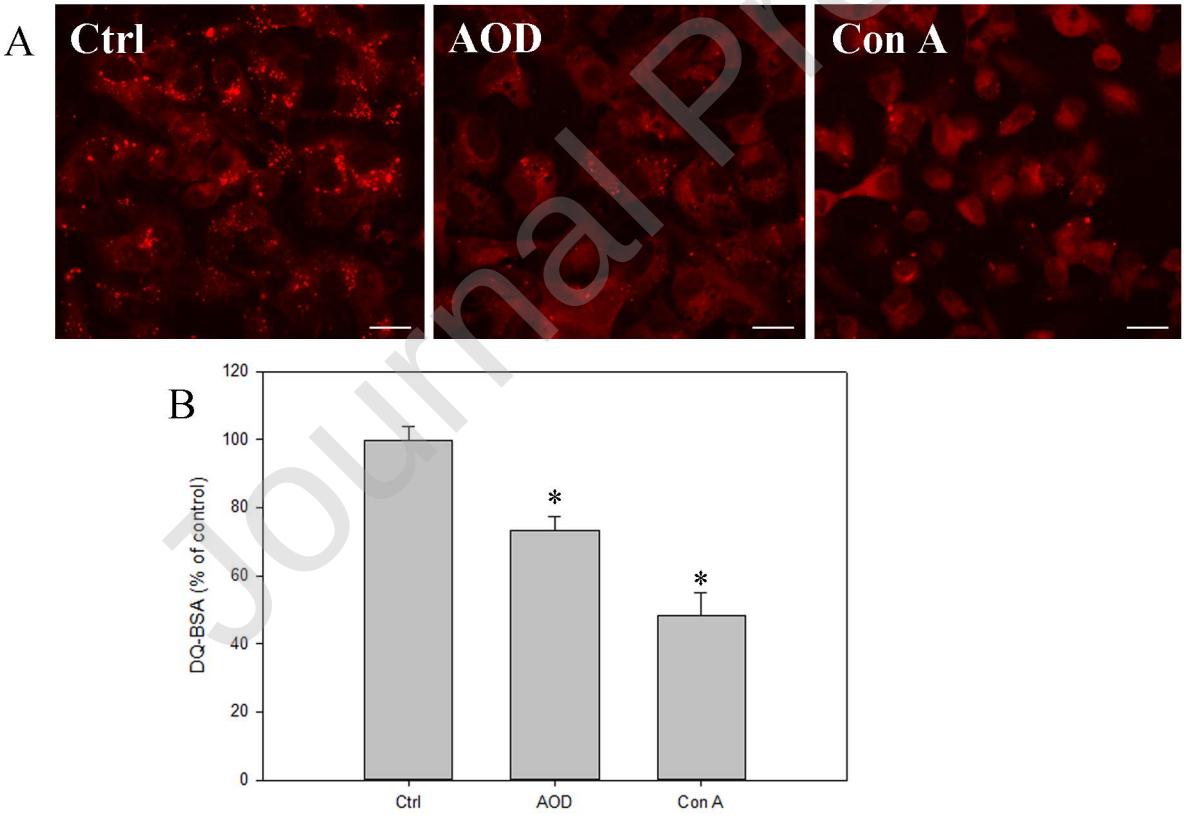
A
Ctrl
AOD
Con A
B
DQ-BSA (% of control)
120
100
80
60
40
20
0
*
*
Ctrl
AOD
Con A

A

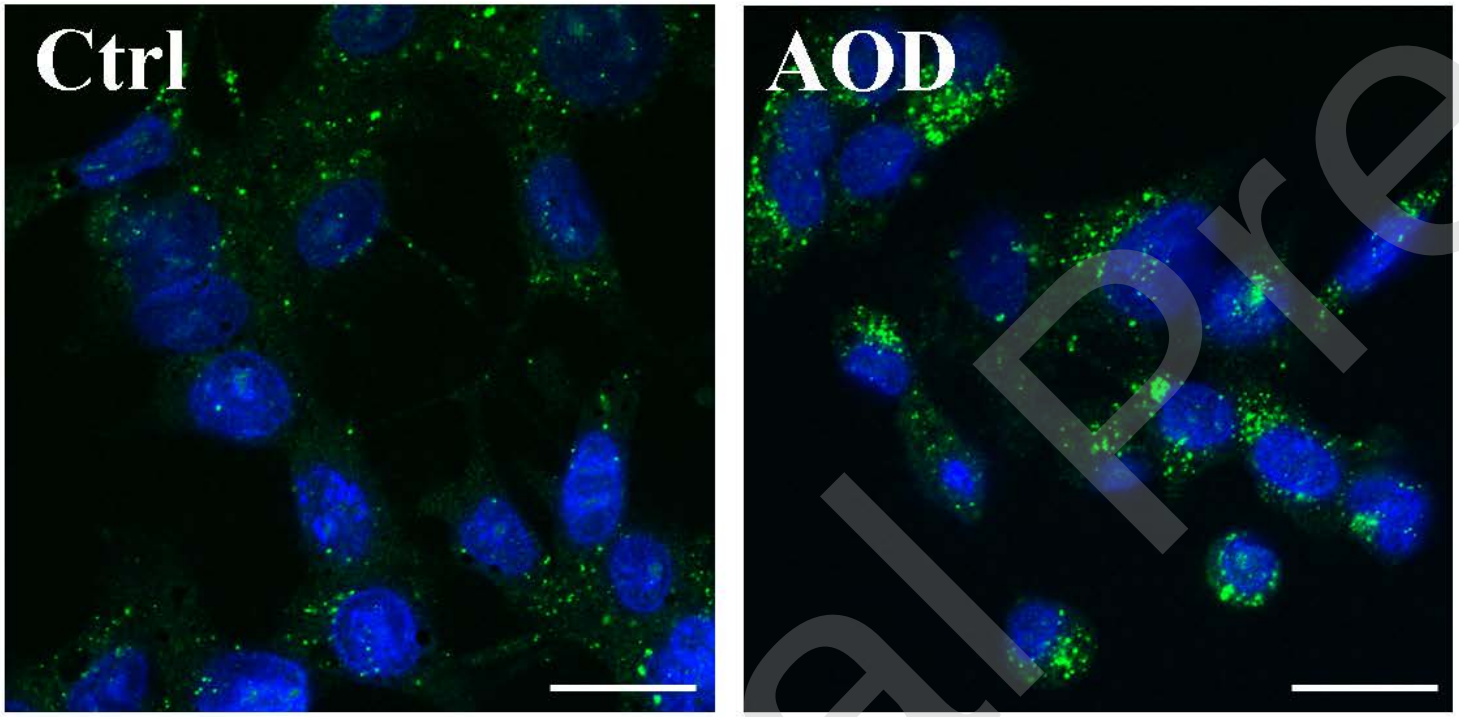

B

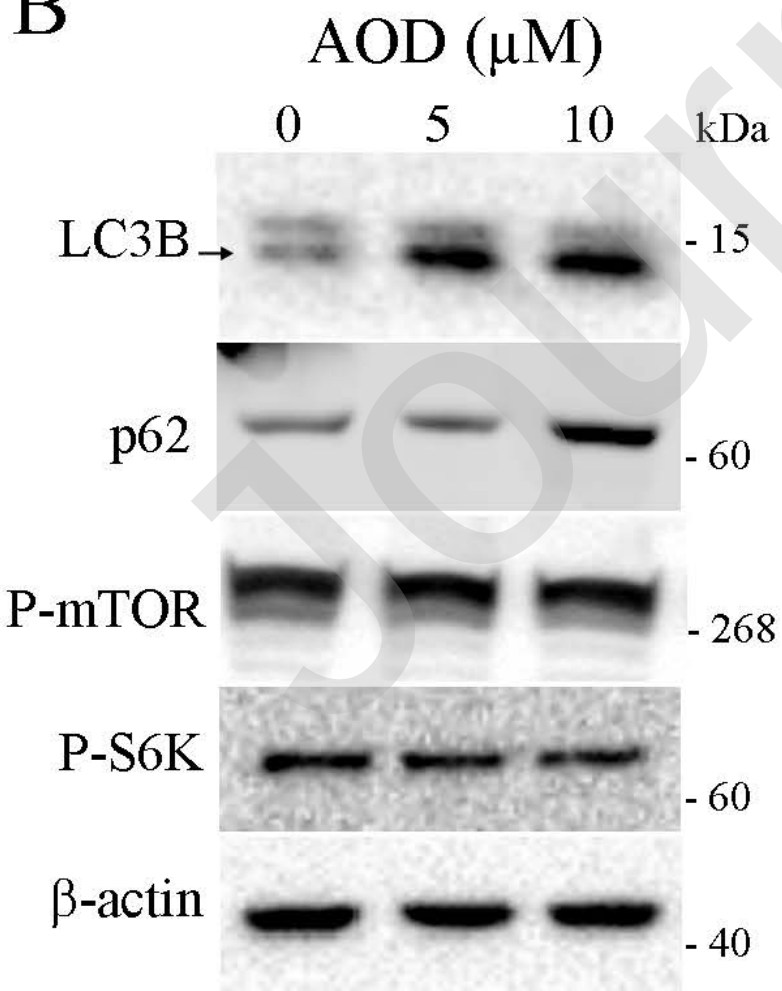

C

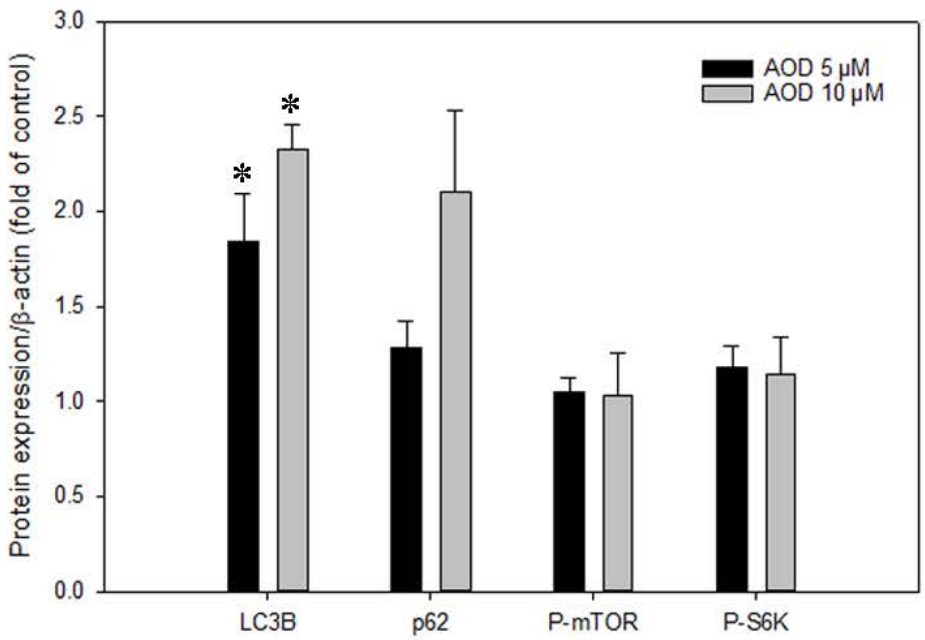

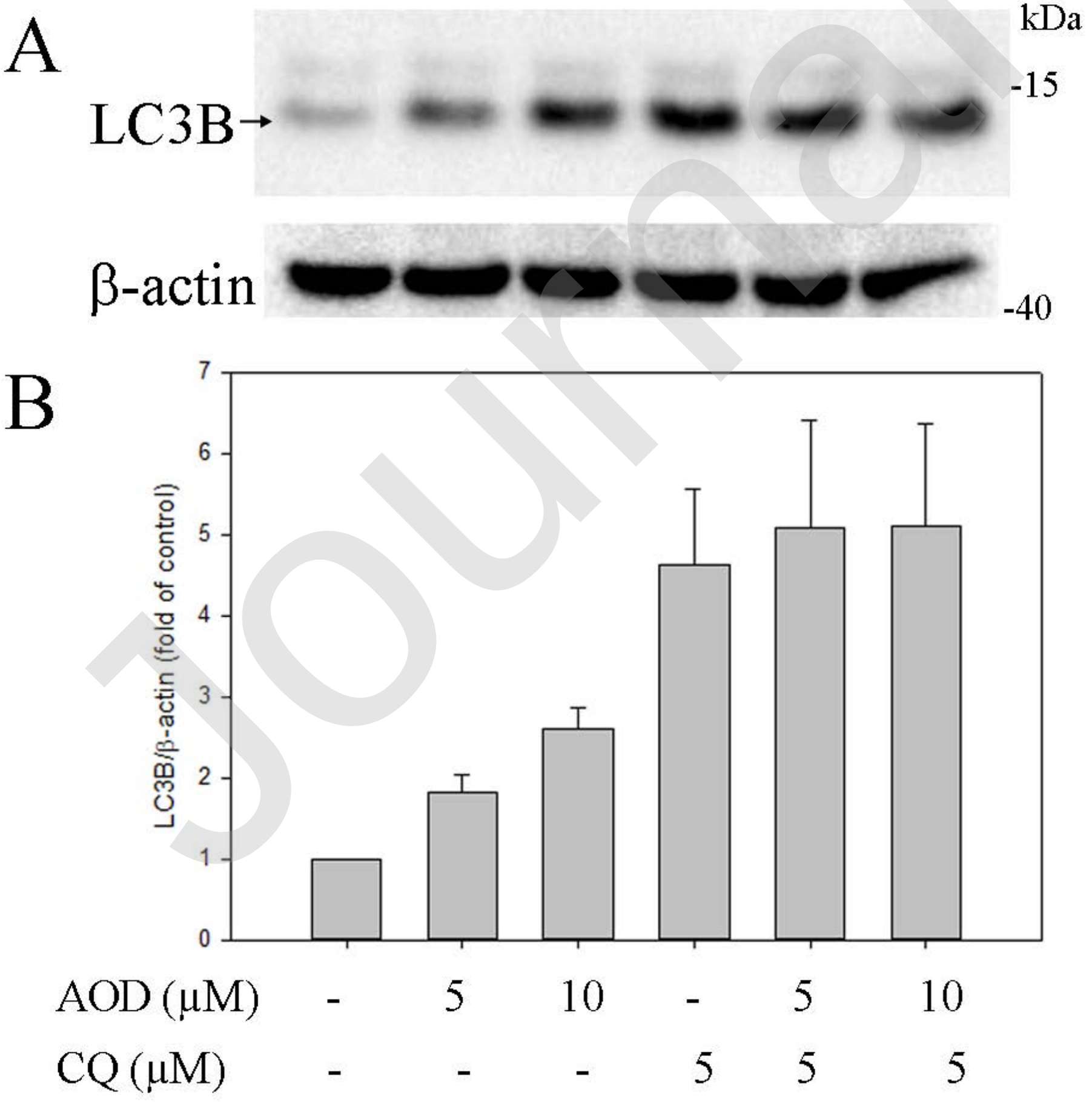
A
kDa
-15
LC3B
β-actin
-40
B
LC3B/β-actin (fold of control)
0
1
2
3
4
5
6
7
AOD (μM) - 5 10 - 5 10
CQ (μM) - - - 5 5 5

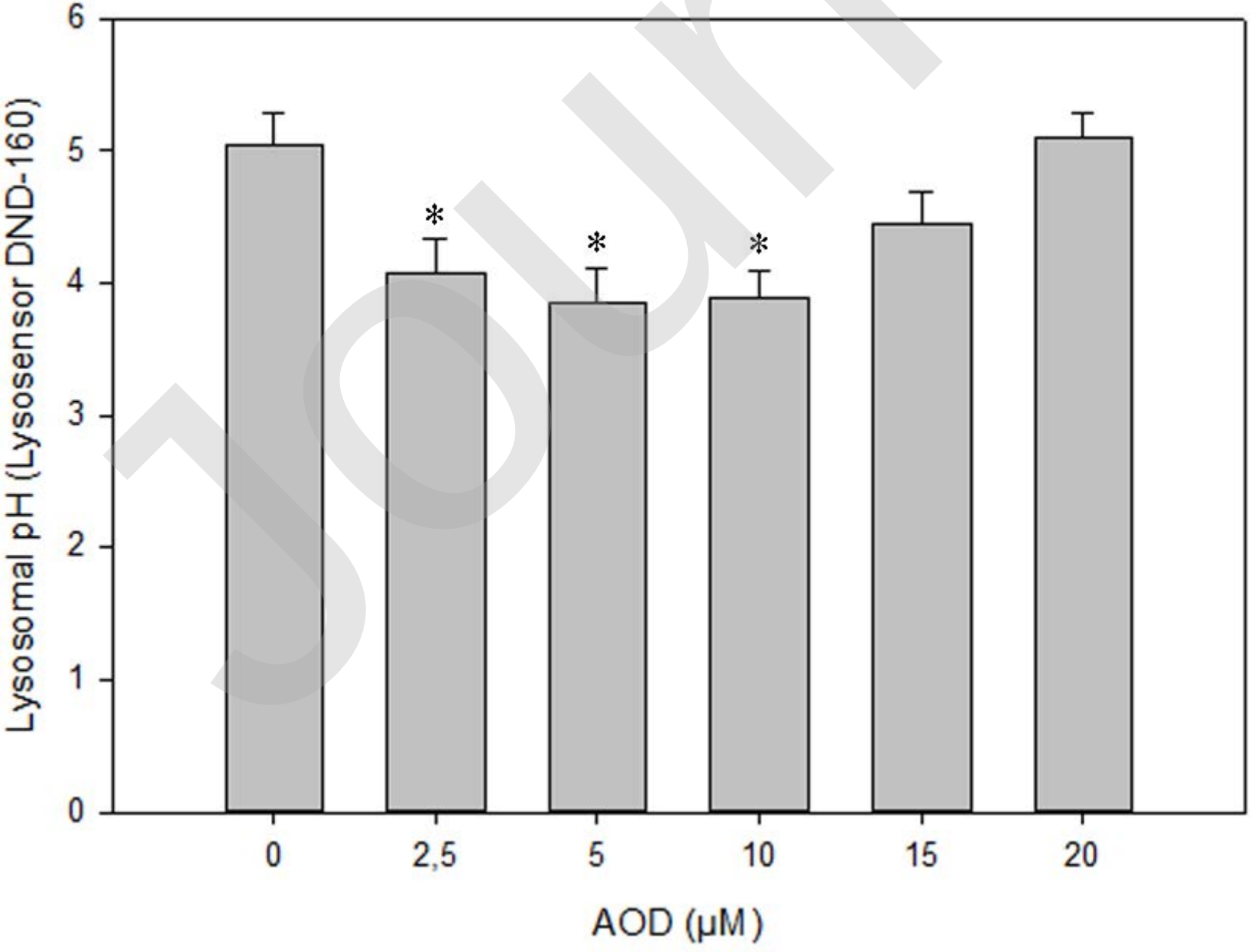
Lysosomal pH (Lysosensor DND-160)
6
5
4
3
2
1
0
*
*
*
0
2,5
5
10
15
20
AOD (μM)